Hindawi Publishing Corporation
Journal of Nanomaterials
Volume 2012, Article ID 905178, 5 pages
doi:10.1155/2012/905178

Research Article

Freestanding Ge/GeO_2 Core-Shell Nanocrystals with Varying Sizes and Shell Thicknesses: Microstructure and Photoluminescence Studies

P. K. Giri[1,2] and Soumen Dhara[1]

[1] *Department of Physics, Indian Institute of Technology Guwahati, Guwahati 781039, India*
[2] *Centre for Nanotechnology, Indian Institute of Technology Guwahati, Guwahati 781039, India*

Correspondence should be addressed to P. K. Giri, pravat_g@yahoo.com

Received 31 May 2011; Accepted 30 June 2011

Academic Editor: Linbao Luo

Freestanding Ge/GeO_2 core-shell nanocrystals (NCs) with varying sizes and shell thicknesses were synthesized by a ball milling method. The core-shell NCs consist of single crystalline Ge core and crystalline GeO_2 shell. With increasing milling time, sizes of the NCs decrease while GeO_2 shell layer thicknesses increase. After 30 hours of milling, size of the core-shell NCs goes down to 11 nm. Analysis of high-resolution transmission electron microscope images revealed the presence of strain in the NCs and lattice distortion/dislocations in the Ge core near the interface of Ge core and GeO_2 shell. This induced a strong phonon localization effect as evident from Raman studies and leads to enhanced radiative recombination, resulting in intense photoluminescence. Strong photoluminescence peaks in the visible and UV region were observed from all the samples and are attributed to Ge/GeO_2 interface defect states. Optical Raman scattering studies confirm the formation of strained Ge/GeO_2 core-shell NCs with varying thicknesses.

1. Introduction

Nanocrystals (NCs) of indirect-gap semiconductors like Si and Ge are widely studied as they open new possibilities for applications as a building block in the optoelectronics and microelectronics [1–3]. As the exciton Bohr radius of Ge (24.3 nm) [4] is much larger than Si (4.9 nm) [5], the quantum confinement effect and hence the enhancement of bandgap are more prominent in Ge NCs. The optical properties, for example, photoluminescence (PL) in the UV-Vis region from of the isolated Ge NCs or Ge NCs embedded in SiO_2 matrix or Ge/GeO_2 core-shell NCs have been reported earlier [2, 6–10]. It is found that light emission is more prominent in the case of Ge/GeO_2 core-shell NCs. The light emission mechanism has been explained on the basis of radiative recombination via Ge quantum confined or due to interface defects at the nanocrystal/matrix or in the matrix itself. The role of interface in both passivating nonradiative states and in the formation of radiative states is also reported to be quite significant. Now it is generally accepted that both localized defect states at the interface and quantum confinement of excitons due to size reduction have combined contributions toward UV-Vis PL from Ge NCs/GeO_2 core-shell system. It is difficult to isolate the relative contributions of interfacial defects and size, as the interfacial defect-related PL itself depends on size [11, 12]. In most of the studies the Ge or Ge/GeO_2 NCs were synthesized by high temperature annealing. Such high temperature processing is not compatible for the fabrication of electronic devices and also it can degrade the device performance. Recently, Tsai et al. [13] synthesized Ge NCs embedded in GeO_x film at low temperature without postannealing by using CO_2 laser-assisted chemical vapour deposition technique and studied its microstructure and light emission property. Here we synthesized isolated freestanding Ge/GeO_2 core-shell NCs with varying shell thicknesses by employing simple mechanical ball milling. Microstructure was analysed by X-ray diffraction (XRD) and transmission electron microscope

(TEM) and correlate the influence of shell-NCs interface on the observed PL in the UV-Vis region.

2. Experimental Details

The freestanding Ge NCs were prepared from high purity (99.999%) Ge powder by mechanical milling in a planetary ball mill for the duration of 5–30 h. The Ge powder was milled in a zirconium oxide vial with small balls of zirconium oxide. This ensures that no metallic contaminants are introduced during the milling process. The milling was performed under normal atmospheric conditions with presence of air to enable the formation of oxide shell layer over the NCs. The nanopowder samples obtained for different hours of milling were studied by high resolution X-ray diffraction (XRD) measurements (Bruker, Advance D8) in a slow scan mode. A 200 KV HRTEM (JEOL-2100) was used to study the size and the microstructure of the freestanding NCs. The UV-Visible absorption spectra of all the samples were recorded using a commercial spectrometer (Shimadzu 3010PC). The PL spectra of the freestanding core-shell Ge NCs for different milling hours were recorded (Jobin-Yvon, T64000) with an excitation of 325nm laser. Raman scattering measurement was carried out with a 488 nm Ar^+ laser excitation using a micro-Raman spectrometer (LabRam HR800) equipped with a liquid nitrogen cooled charge coupled device (CCD) detector. Fourier transformed infrared spectroscopy (FTIR, Perkin Elmer, Spectrum BX) was used to check the chemical bonding configuration of the NCs. For discussion, we denote the unmilled, 5 h, 10 h, 20 h, 25 h, and 30 h milled Ge NCs samples as Ge-0, Ge-5, Ge-10, Ge-20, Ge-25, and Ge-30, respectively.

3. Results and Discussion

Figure 1(a) shows the TEM image of an isolated Ge/GeO_2 NC for the Ge-10 sample. The variation in contrast at the edge of the NCs (region marked with hollow arrow) indicates the presence of GeO_2 shell layer over the Ge core. Figures 1(b)–1(d) show the core-shell NCs for the Ge-20, Ge-25, and Ge-30 samples, respectively. With increase in milling time, the size of the NCs gradually decreases and after 30h of milling, average size of the NCs is 11 nm. The size obtained from the TEM images is the diameter of the core-shell NCs, whereas XRD gives the average size of the Ge core in the Ge/GeO_2 core-shell NCs. Therefore extraction of sizes obtained from TEM imaging by the sizes obtained from the XRD line profile analysis can give the estimated thickness of the shell in the core-shell NCs. In this case, we calculated the GeO_2 shell thickness in the Ge/GeO_2 NCs. It is found that shell thickness gradually increases from 0.5 nm to 1.5 nm for the milled time duration 10 h to 30 h. From Ge-5 to Ge-30, the sizes of the NCs are smaller than the exciton Bohr diameter of bulk Ge. Therefore, one would expect enhanced PL from all the samples. Insets of Figures 1(b) and 1(d) show the inverse fast Fourier transformed (FFT) lattice images of the isolated NC for the Ge-20 and Ge-30, respectively. One can clearly see the presence of lattice dislocation/distortion (region marked with solid arrow) induced defect states near

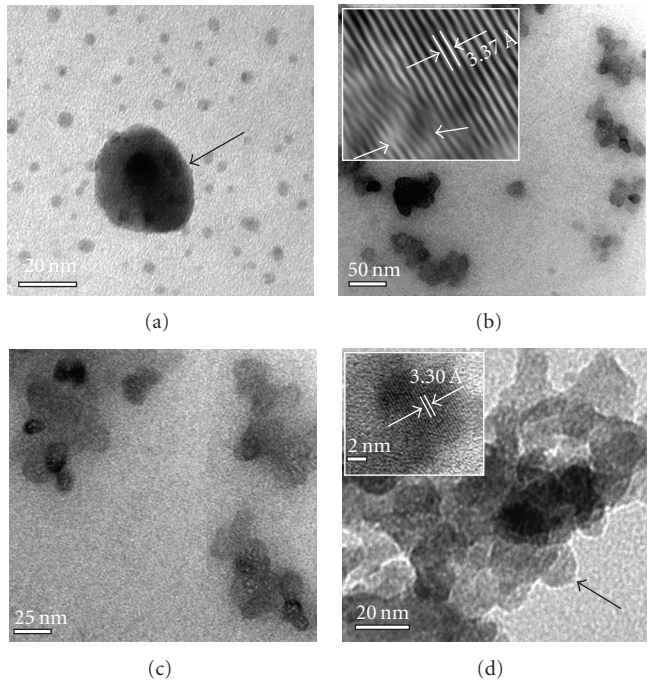

Figure 1: TEM images for the Ge-10, Ge-20, Ge-25, and Ge-30 NCs. Insets of (b) and (d) show the high-resolution lattice image of the Ge NCs core for the Ge-20 and Ge-30, respectively.

the grain boundary between Ge core and GeO_2 shell. The lattice spacing of the Ge core for the Ge-20 sample is calculated to be 3.37 Å, which corresponds to the (111) plane of Ge with diamond cubic structure. The calculated lattice spacing is larger than the lattice spacing of unstrained Ge (3.27 Å). This confirms that tensile strain is indeed present in the core-shell NCs. For the Ge-30 sample, it is found that lattice spacing reduced to 3.30 Å, which indicates a relaxation of lattice strain. These results are consistence with the XRD results. It is known that high densities of structural defects could lead to the phonon localization effects [14], therefore, one would expect enhanced PL properties form the ultra small and strained Ge/GeO_2core-shell NCs due to combined effects of quantum confinement and phonon localization.

Figure 2 shows the XRD pattern of the freestanding Ge/GeO_2 core-shell NCs milled for different time durations. Along with the strong Ge(111) peak, GeO_2-related XRD peaks are also observed. With the increase in milling time, the intensities of the Ge(111) peak decrease, while intensities of GeO_2(101) peak increase. The intensity ratio of GeO_2(101) to the Ge(111) peak increases from 0.6 to 3.2. The observed intensity enhancement for the GeO_2(101) peak clearly indicates that thickness of GeO_2 layer increases with increasing milling time, while the size of the Ge NCs reduces accordingly. The XRD results clearly show the formation of Ge/GeO_2core-shell NCs with varying thicknesses. The d spacing of Ge(111) core increases with increasing milling time up to 20 h of milling as found from shift in 2θ value. This increase in lattice spacing indicates the presence of tensile strain in the NCs, which increases with increase in shell thickness. The exact sizes of the Ge core in the Ge/GeO_2

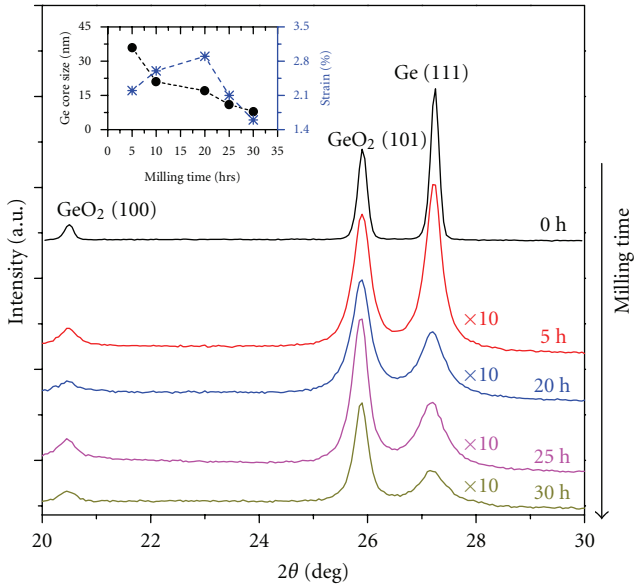

FIGURE 2: XRD patterns of the freestanding Ge/GeO_2 core-shell NCs milled for different time duration. Intensity of the GeO_2(101) peak increases systematically with increasing milling time.

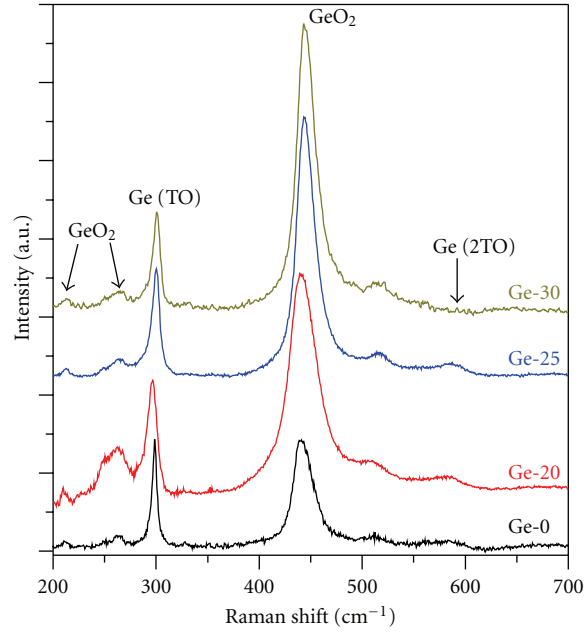

FIGURE 3: Raman spectra of the Ge/GeO_2 core-shell NCs obtained after different milling times. With increase in milling time, Raman peak intensity of GeO_2 increases while Raman peak intensity of Ge decreases.

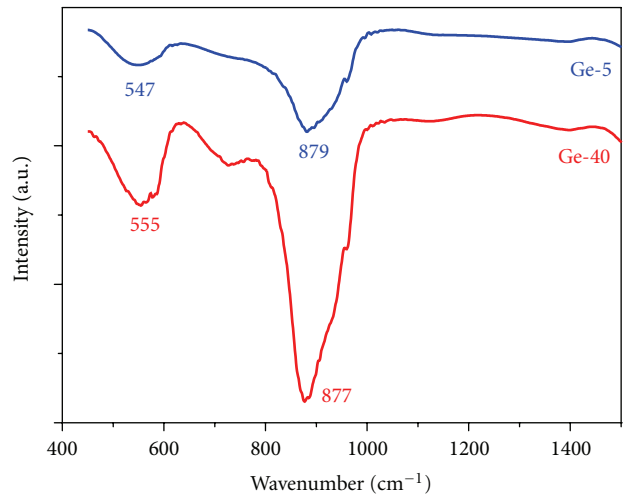

FIGURE 4: FTIR spectra for the Ge-5 and Ge-30 samples. Various Ge-O vibrational modes are labelled with corresponding wave numbers.

NCs and the lattice strain are calculated by detailed analysis of XRD line profile. The method proposed by Ungar and Borbely [15] is used to calculate the exact Ge core size and lattice strain of the GeO_2NCs. According to the Ungar and Borbely method, individual contribution of size and strain to the broadening can be expressed as

$$\Delta K = \frac{0.9}{D_U} + 2eK\sqrt{C}, \quad (1)$$

where $\Delta K = (2\beta \cos\theta_B)/\lambda$, β is the FWHM (in radians) of the Bragg reflections, θ is the Bragg angle of the analyzed peak, λ is the wavelength of X-rays, D_U is the average crystallite size, $K = 2 \sin\theta_B/\lambda$, e is the strain, and C is the dislocation contrast factor, respectively. Details of the above calculation for Ge NCs can be found elsewhere [16]. The Sizes of the Ge core and lattice strain calculated from the above method are shown as inset of Figure 2. With increase in milling time size of the Ge core gradually decreases from 36 nm to 8 nm for 5 h to 30 h samples. On the other hand, the strain first increases up to 20 hours of milling (maximum strain ~2.9%) and then it decrease for higher milling time. This strain reduction indicates the release of tensile strain in the Ge/GeO_2 NCs. This can be explained as follows: during milling the strain and dislocations first develop, however for prolonged milling when the dislocation density is high the crystal breaks along the slip plane and thus produces smaller size NCs. In this way, NC size is reduced and strain is partly released for prolonged milling time [16].

The crystalline quality of the Ge/GeO_2 core-shell NCs and lattice strain was further studied by micro-Raman analysis, which is shown in Figure 3 for various samples. The Ge-0 sample exhibits a sharp peak at 298.5 cm^1 with FWHM of 5.4 cm^1 and a weak hump at ~570 cm^1. These two modes are attributed as the well-known Raman active first-order and second-order transverse optical (TO) phonon mode of crystalline Ge [17]. Along with the TO modes of Ge, additional three modes are observed from all the samples at ~212 cm^1, ~261 cm^1, and ~440 cm^1. These three modes are the characteristic Raman active modes of crystalline GeO_2 [18]. With increase in milling times, the intensity ratio of strongest GeO_2 Raman mode to the Ge(TO) mode increases gradually from 1.01 to 2.65. This indicates the increase of shell layer thickness from Ge-0 to Ge-30. These results are consistent with the XRD results, discussed earlier. From Ge-0 to Ge-20, the TO modes of Ge shows gradual redshift from 298.5 to

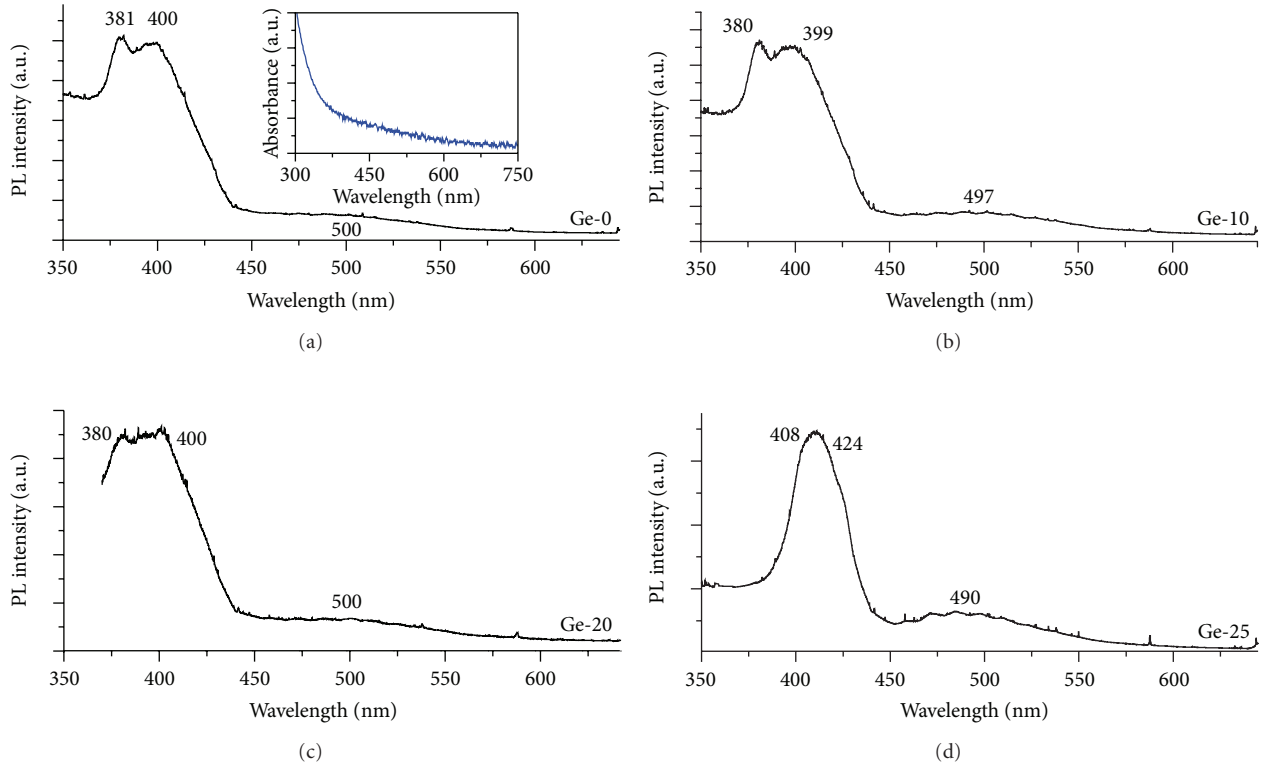

Figure 5: Room temperature PL spectra for the Ge-0, Ge-10, Ge-20, and Ge-25. Inset of (a) shows the absorption spectra of the corresponding Ge/GeO_2 NCs.

296.3 cm^1 and FWHM increases from 5.4 to 11.7 cm^1. The observed redshift is due to the combined effects of phonon confinement and tensile strain, as both the effects result in redshift in the Raman modes [19, 20]. The line width broadening is caused by size distribution of Ge NCs and phonon confinement effect in the Ge NCs. The Raman line width is known to be inversely proportional to the size of the NCs. With further milling, TO modes of Ge are blueshifted due to decrease in tensile strain by lattice relaxation. Here, observed blueshift results from the reduced tensile strain and this is consistent with the XRD analysis.

FTIR spectroscopy was employed further to investigate the chemical bonding configuration of the core-shell Ge/GeO_2 NCs. Figure 4 shows the FTIR spectra for the Ge-5 and Ge-40 samples. Two intense broad bands are observed from all the samples. The bands at 5472 cm^1 and 555 cm^1 correspond to the Ge-O-Ge bending modes while the bands at 879 cm^1 and 877 cm^1 correspond to Ge-O-Ge stretching modes of GeO_2, respectively [21]. These oxide species stem from the oxide shell layer on the Ge core.

Figure 5 shows the room temperature PL spectra for Ge-0, Ge-10, Ge-20, and Ge-25 samples. From Ge-0 to Ge-30, all the samples show strong peaks in the UV region as well as weak peak in the visible region. The UV-Vis absorption spectrum of the Ge-0 sample is shown as inset in Figure 5(a). The absorption spectrum shows strong absorption in the UV region and a weak absorption in the visible region. Other samples show similar absorption spectra with varying intensities. Two PL emission peaks in the UV-violet region (~380–400 nm) and one peak in the green region(~500 nm) were observed from all the samples. Note that as compared to other samples, Ge-25 shows a redshift in the UV-violet peaks with PL peaks at 408 and 424 nm. Though exact mechanism of this redshift is not clear, this might be related to the relaxation of strain in the Ge-25. In all the samples, PL spectra have similar features and peak positions are nearly independent of sizes of Ge NCs. And direct recombination in GeO_2 results in PL emission below 250 nm [22]. Thus, the observed PL does not originate from the radiative recombination of excitons confined in the Ge or GeO_2 NCs. Therefore, first PL component may originate from dislocation related defects at the Ge core and GeO_2 boundary, as intensity of the first component systematically increases from Ge-0 to Ge-20. Note that, dislocation-related defect density gradually increases from Ge-0 to Ge-20. The high density of defects due to lattice dislocation/disorder, located in surface and grain boundaries of the NCs induced a significant localisation effect resulting in strong PL. The ~400 nm peak is attributed to Ge/O stoichiometric defect states at the interface [23]. As the milling was done in sealed vial, it is expected to form Ge/O stoichiometric defect states in NCs. The ~500 nm peak is originated from radiative recombination between the oxygen vacancies and oxygen-germanium vacancy centers [24]. No observable visible PL emission is observed from Ge NCs core, perhaps due to large strain that causes nonradiative recombination centres to quench the PL.

4. Conclusions

We have synthesized freestanding Ge/GeO_2core-shell NCs with size down to 11 nm with varying shell thicknesses (up to 1.5 nm) by ball milling method. Analysis of HRTEM images and XRD patterns revealed the presence of lattice strain in the Ge core near the interface between Ge and GeO_2 and the nature of strain is tensile. With increase in milling time, lattice stain initially increases up to 20 hours of milling then partially released for further milling. The Raman scattering studies shows that observed redshift in the Raman modes results from the combined effect of quantum confinement and tensile strain. High densities of structural defects (lattice dislocation/distortion) in the synthesized NCs result in enhanced PL in the UV and visible region and are attributed to various Ge/GeO_2 interface defects. No observable visible PL emission is observed from Ge NCs core, perhaps due to large strain that causes nonradiative recombination centres to quench the PL.

References

[1] T. C. Tsai, L. Z. Yu, and C. T. Lee, "Electroluminescence emission of crystalline silicon nanoclusters grown at a low temperature," *Nanotechnology*, vol. 18, no. 27, Article ID 275707, 2007.

[2] Y. Maeda, "Visible photoluminescence from nanocrystallite Ge embedded in a glassy SiO_2 matrix: evidence in support of the quantum-confinement mechanism," *Physical Review B*, vol. 51, no. 3, pp. 1658–1670, 1995.

[3] C. L. Yuan and P. S. Lee, "Enhanced charge storage capability of Ge/GeO_2 core/shell nanostructure," *Nanotechnology*, vol. 19, no. 35, Article ID 355206, 2008.

[4] Y. Maeda, N. Tsukamoto, Y. Yazawa, Y. Kanemitsu, and Y. Masumoto, "Visible photoluminescence of Ge microcrystals embedded in SiO_2 glassy matrices," *Applied Physics Letters*, vol. 59, no. 24, pp. 3168–3170, 1991.

[5] A. G. Cullis, L. T. Canham, and P. D. J. Calcott, "The structural and luminescence properties of porous silicon," *Journal of Applied Physics*, vol. 82, no. 3, pp. 909–966, 1997.

[6] X. Ma, W. Shi, and B. Li, "The size dependence of the optical and electrical properties of Ge quantum dots deposited by pulsed laser deposition," *Semiconductor Science and Technology*, vol. 21, no. 5, pp. 713–716, 2006.

[7] P. K. Giri, S. Bhattacharyya, S. Kumari et al., "Ultraviolet and blue photoluminescence from sputter deposited Ge nanocrystals embedded in SiO_2 matrix," *Journal of Applied Physics*, vol. 103, no. 10, Article ID 103534, 9 pages, 2008.

[8] S. Takeoka, M. Fujii, S. Hayashi, and K. Yamamoto, "Size-dependent near-infrared photoluminescence from Ge nanocrystals embedded in SiO_2 matrices," *Physical Review B*, vol. 58, no. 12, pp. 7921–7925, 1998.

[9] P. K. Sahoo, S. Dhar, S. Gasiorek, and K. P. Lieb, "Stable violet cathodoluminescence of α-quartz after Ge^+ implantation at elevated temperature," *Journal of Applied Physics*, vol. 96, no. 3, pp. 1392–1397, 2004.

[10] C. L. Yuan and P. S. Lee, "Enhancement of photoluminescence of Ge/GeO_2 core/shell nanoparticles," *Europhysics Letters*, vol. 83, no. 4, Article ID 47010, 5 pages, 2008.

[11] X. X. Wang, J. G. Zhang, L. Ding et al., "Origin and evolution of photoluminescence from Si nanocrystals embedded in a SiO_2 matrix," *Physical Review B*, vol. 72, no. 19, Article ID 195313, 6 pages, 2005.

[12] G. Hadjisavvas and P. C. Kelires, "Structure and energetics of Si nanocrystals embedded in a-SiO_2," *Physical Review Letters*, vol. 93, no. 22, Article ID 226104, 4 pages, 2004.

[13] T.-C. Tsai, D.-S. Liu, L.-R. Lou, and C.-T. Lee, "Structure and photoluminescence of Ge nanoclusters embedded in GeO_x films deposited using laser assistance at low temperature," *Journal of Applied Physics*, vol. 108, no. 7, Article ID 074318, 4 pages, 2010.

[14] N. H. Nickel, P. Lengsfeld, and I. Sieber, "Raman spectroscopy of heavily doped polycrystalline silicon thin films," *Physical Review B*, vol. 61, no. 23, pp. 15558–15561, 2000.

[15] T. Ungar and A. Borbely, "The effect of dislocation contrast on x-ray line broadening: a new approach to line profile analysis," *Applied Physics Letters*, vol. 69, no. 21, pp. 3173–3175, 1996.

[16] P. K. Giri, "Strain analysis on freestanding germanium nanocrystals," *Journal of Physics D*, vol. 42, no. 24, Article ID 245402, 7 pages, 2009.

[17] Z. Sui and I. P. Herman, "Effect of strain on phonons in Si, Ge, and Si/Ge heterostructures," *Physical Review B*, vol. 48, no. 24, pp. 17938–17953, 1993.

[18] S. Tsutomu and S. L. Jun, "Lattice dynamics and temperature dependence of the linewidth of the first-order Raman spectra for sintered hexagonal GeO_2 crystalline," *Journal of the Physical Society of Japan*, vol. 67, no. 11, pp. 3809–3815, 1998.

[19] R. Jalilian, G. U. Sumanasekera, H. Chandrasekharan, and M. K. Sunkara, "Phonon confinement and laser heating effects in Germanium nanowires," *Physical Review B*, vol. 74, no. 15, Article ID 155421, 6 pages, 2006.

[20] Y. Y. Fang, J. Tolle, R. Roucka et al., "Perfectly tetragonal, tensile-strained Ge on $Ge_{1-y}Sn_y$ buffered Si(100)," *Applied Physics Letters*, vol. 90, no. 6, Article ID 061915, 3 pages, 2007.

[21] M. Ardyanian, H. Rinnert, and M. Vergnat, "Influence of hydrogenation on the structure and visible photoluminescence of germanium oxide thin films," *Journal of Luminescence*, vol. 129, no. 7, pp. 729–733, 2009.

[22] D. M. Christie and J. R. Chelikowsky, "Electronic and structural properties of germania polymorphs," *Physical Review B*, vol. 62, no. 22, pp. 14703–14711, 2000.

[23] M. Zacharias and P. M. Fauchet, "Blue luminescence in films containing Ge and GeO_2 nanocrystals: the role of defects," *Applied Physics Letters*, vol. 71, no. 3, pp. 380–382, 1997.

[24] X. C. Wu, W. H. Song, B. Zhao, Y. P. Sun, and J. J. Du, "Preparation and photoluminescence properties of crystalline GeO_2 nanowires," *Chemical Physics Letters*, vol. 349, no. 3-4, pp. 210–214, 2001.